High-order harmonic generation of 1-nonene under linearly polarized laser pulses

Shu-Shan Zhou,[1,2] Wen-Di Lan,[1,2] Ji-Gen Chen,[3] Jun Wang,[1,2,*] Fu-Ming Guo,[1,2,†] and Yu-Jun Yang[1,2,‡]
[1]*Institute of Atomic and Molecular Physics, Jilin University, Changchun 130012, China*
[2]*Jilin Provincial Key Laboratory of Applied Atomic and Molecular Spectroscopy (Jilin University), Changchun 130012, China*
[3]*Zhejiang Provincial Key Laboratory for Cutting Tools, Taizhou University, Jiaojiang 318000, China*

(Received 18 July 2021; revised 28 June 2022; accepted 18 July 2022; published 11 August 2022)

High-order harmonic generation of the long-chain molecule 1-nonene (C_9H_{18}) under a few-cycle linearly polarized laser field was studied using time-dependent density-functional theory. The efficiency and the cutoff frequency of the C_9H_{18} harmonic spectrum are significantly higher than those of the BF molecule irradiated by the same laser pulse. By analyzing the time-frequency behavior of the harmonic and the classical simulation of electron, it is found that the C_9H_{18} harmonics near the cutoff energy are caused by the recombination of electrons from one atom to others of the parent molecule. In addition, the high-order harmonic generation of the long-chain molecule 1,3-Butadiene (C_4H_6) is also investigated. The harmonics generated by this mechanism can be applied to produce high-intensity isolated attosecond pulses.

DOI: 10.1103/PhysRevA.106.023510

I. INTRODUCTION

Atoms, molecules, and solids irradiated by an intense laser pulse can lead to a variety of strong field physical phenomena, such as tunneling ionization [1], above-threshold ionization [2], nonsequential double ionization [3,4], Coulomb explosion [5,6], high-order harmonic generation (HHG) [7–16], and so on. The HHG generated by an intense laser pulse is one of the main ways to obtain the table-top level coherent radiation source in the extreme ultraviolet (XUV) and soft x-ray region [17]. At the same time, due to the wide spectrum of the harmonic spectrum, the ultrashort pulse generated by it provides an effective way for monitoring and controlling electron dynamics on the attosecond (1 as $= 10^{-18}$ s) [18–22] timescale resolution and Ångström (1 Å $= 10^{-10}$ m) space scale resolution. At present, the harmonic intensity is low and its spectral range is not wide enough, which limits the further application of HHG.

The mechanism of the atomic HHG is usually explained by the semi-classical three-step model (TSM) [23]: under the interaction of the laser electric field, the bound electrons are freed by tunneling ionization, then some ionized electronic wave packets have the opportunity to return to the parent ions, and they recombine with the parent ions to generate the high-energy photon.

Compared with the atom, the molecular structure is more complex and the ionization energies of different molecular orbitals are closer, so the molecular HHG is more complex. For the mechanism of the molecular HHG, extensive and in-depth research has been done in theory and experiment before. In the case of the molecule with a smaller spatial scale, the ionized electrons can return to the parent nucleus or adjacent one to cause interference. For diatomic molecules with homonuclear [24–29] or heteronuclear [27,30,31], and simple molecules with polyatomic [32–36], the harmonic spectrum is different from the atomic HHG spectrum. Irani *et al.* studied the harmonic spectrum of the Br_2 molecule to generate multiplateau and expand the harmonic plateau by adjusting the carrier-envelope phase (CEP) and the molecular orientation [29]. Monfared *et al.* found that multiorbitals of the molecule N_2O contribute to the harmonic spectrum, and the tunneling ionization of HOMO-1 electrons leads to the cutoff extension [35]. Yun *et al.* extended the harmonic spectrum of the molecule CO_2 in an intense laser field by using an orthogonal two-color field [37].

For the HHG of molecules with a more complex structure or larger spatial scale in the strong field, due to its complexity, the in-depth research is relatively less. Altucci *et al.* proved that the specific hydrocarbon molecular orbital has an important effect on the nonaligned polyatomic molecular HHG [38]. By constructing a suitable mixture of *s*-type and *p*-type atomic wave functions, an excellent agreement between measurements and simulations in methane is found, and confirmed the important role played by the *p*-like character originating from the covalent C-H bond. Torres *et al.* and Kajumba *et al.* investigated the dependence of the harmonic yield on the angle between the polarization of the driving laser field and the axis of aligned polyatomic molecules such as acetylene and propane. It was demonstrated that the measured results were in good quantitative agreement with the calculated results using the strong field approximation, indicating that the angle-dependent spectrum carried the information about the molecular orbital structure and the symmetry [39,40]. Vozzi *et al.* studied the influence of the specific molecular orbital in HHG by aligned polyatomic molecules for ethane (C_2H_6), acetylene (C_2H_2), propane (C_3H_8), butane (C_4H_{10}), ethylene (C_2H_4), allene (C_3H_4), and 1,3-butadiene. The spectra were

*wangjun86@jlu.edu.cn
†guofm@jlu.edu.cn
‡yangyj@jlu.edu.cn

modulated by different alignment angles and showed signatures of the molecular structure [41]. Zhu *et al.* examined the anomalous circular dichroism of HHG for three isomers of the 6.4 stereo-molecular tartaric acid under the circularly polarized laser pulse [42]. Yuan *et al.* investigated the HHG of molecules with enlarged nuclear distances in a circularly polarized laser field, and they demonstrated that the energy exchange between electrons caused by double ionization can expand the harmonic spectrum [43]. Lein *et al.* also studied the HHG of molecules with enlarged nuclear distances in the linearly polarized laser field, and they affirmed that the maximum kinetic energy produced by collisions with adjacent ions is $I_P + 8U_P$, which is higher than the maximum of the linearly polarized recollision [44,45]. The above research shows that it is possible to use the molecular HHG to enhance the harmonic efficiency and increase the cutoff frequency.

However, for complex molecules with larger spatial scales, due to their polyatomic characteristics and larger spatial distribution, their harmonic emission process under the ultrashort pulse is more complicated, and there are fewer relevant studies up to now. Sansone *et al.* synthesized isolated attosecond pulses using the polarization gate technique, based on the concept of the quantum path, and discussed the influence of the driving pulse with the amplitude and the CEP on harmonic spectral characteristics [46]. Calegari *et al.* depended on the CEP of the driving field, obtained complete control of the XUV emission over the entire spectral range, and isolated or multiple attosecond pulses were produced by the quantum path control mechanism [47]. In this study, time-dependent density-functional theory (TDDFT) is used, and the time-frequency analysis of the harmonic emission can be combined with the classical trajectory to explain the cutoff position of the harmonic spectrum. Due to the lack of the phase information in classical trajectories, a quantitative explanation for quantum interference effects caused by different emission mechanisms cannot be obtained. For complex molecules with a larger spatial scale driven by an ultrashort laser, more molecular orbitals will contribute to the ionization and recombination processes, and the recombination spatial area is not limited to the vicinity of the tunneled atomic nucleus. Compared with the atomic HHG, it is possible to generate the harmonic with higher intensity and greater energy. For this reason, this work theoretically studied the HHG of the long-chain molecule 1-nonene (C_9H_{18}) and 1,3-butadiene (C_4H_6) under the ultrashort laser pulse. In this study, the long axis of the C_9H_{18} molecules is considered aligned with respect to the laser field polarization. It is proved that the cutoff energy and efficiency of the HHG by the interaction of the ultrashort intense laser with the long-chain molecule are higher than that of BF and the enhancement is explained by the time-dependent wave packet motion and the semi-classical simulation.

The organization of this paper is as follows. In Sec. II, the TDDFT is briefly described when the molecular HHG in an intense laser field is simulated. In Sec. III, we give the numerical results of C_9H_{18} harmonic spectra and carry out a detailed analysis and discussion. Our main conclusions are summarized in Sec. IV. Atomic units are used throughout unless otherwise specified.

II. THEORETICAL MODEL AND NUMERICAL METHOD

To simulate the HHG generated by the interaction between ultrashort pulses and molecules, we used the TDDFT method. This scheme is well applicable to the study of HHG generated from the molecule irradiated by the intense laser pulse. The results indicate that the HHG generated from simple diatomic molecules [48], the molecule of benzene [49] and more complex solid-state systems [50] calculated by TDDFT are in good agreement with the experimental measurements. The prediction of HHG by TDDFT calculation can also be verified experimentally [50,51]. In addition, Bedurkes' work suggested that, for the efficiency and cutoff energy of HHG in the complex systems, the simulation results using wave-function theory and TDDFT are consistent [52]. The open-source software package OCTOPUS [53–55], which is based on the evolution of a real-time and real-space grid, was selected for calculations. For a multi-electron system evolving from a given initial state, the Runge-Gross theorem [56] establishes a one-to-one mapping between the time-dependent single-electron density and the time-dependent external potential. The time-dependent electron density of the closed-shell system is

$$\rho(\mathbf{r},t) = 2\sum_{i=1}^{N/2} |\psi_i(\mathbf{r},t)|^2, \tag{1}$$

where i is the orbital index and N is the number of electrons. The single-particle occupation of the Kohn-Sham (KS) orbital $\psi_i(\mathbf{r},t)$ can be obtained from the time-dependent Kohn-Sham (TDKS) equation (in the length gauge)

$$i\frac{\partial}{\partial t}\psi_i(\mathbf{r},t) = \left[-\frac{1}{2}\nabla^2 + V_{\mathrm{KS}}(\mathbf{r},t)\right]\psi_i(\mathbf{r},t), \quad i = 1,\ldots,N. \tag{2}$$

Here $V_{\mathrm{KS}}(\mathbf{r},t)$ is the KS potential

$$V_{\mathrm{KS}}(\mathbf{r},t) = V_{\mathrm{ne}}(\mathbf{r}) + V_{\mathrm{H}}[\rho](\mathbf{r},t) + V_{\mathrm{xc}}[\rho](\mathbf{r},t) + V_{\mathrm{laser}}(\mathbf{r},t), \tag{3}$$

where $V_{\mathrm{ne}}(\mathbf{r})$ is the potential energy that the valence electron feels from the real ion, which is described by the norm-conserved nonlocal Troullier-Martins pseudopotential [57]. The second term $V_{\mathrm{H}}[\rho](\mathbf{r},t)$ is the Hartree potential, which contains the classical Coulomb interaction between electrons,$V_{\mathrm{H}}[\rho](\mathbf{r},t) = \int[\rho(\mathbf{r}',t)/|\mathbf{r}-\mathbf{r}'|]d^3\mathbf{r}'$. The third term $V_{\mathrm{xc}}[\rho](\mathbf{r},t)$ is the exchange-correlation potential, which contains the nonperturbative many-body effect. The parameter used in the exchange-correlation functional is the generalized gradient approximation (GGA) of Perdew-Burke-Ernzerhof [58]. The last term $V_{\mathrm{laser}}(\mathbf{r},t)$ is the interaction between the laser field and the electron.

To realize the time propagation, the density functional theory (DFT) is needed to solve the KS equation to get the initial state. The simulation box with $|\mathbf{r}_x| \leqslant 100$ a.u., $|\mathbf{r}_y| \leqslant 40$ a.u., and $|\mathbf{r}_z| \leqslant 40$ a.u. is used in calculations, and the spacing step is $\Delta\mathbf{r} = 0.4$ a.u.. The approximate enhanced time-reversal symmetry [59] scheme is used to solve the time-dependent KS orbital function, and the time step is $\Delta t = 0.08$ a.u.. To eliminate the nonphysical reflection of the orbital wave function on the boundary, the complex absorption potential (CAP)

[60] is adopted in the simulation

$$V_{\text{absorb}}(r) = \begin{cases} 0, & 0 < r < r_{\max}, \\ i\eta \sin^2\left[\frac{(r-r_{\max})\pi}{2L}\right], & r_{\max} < r < r_m + L, \end{cases} \quad (4)$$

$L = 10$ a.u. and $\eta = -0.8$ a.u. are the width and height of the absorption potential, respectively.

After the time-dependent wave function $\psi_i(\mathbf{r}, t)$ is obtained, the time-dependent dipole moment of the system can be calculated

$$\boldsymbol{d}(t) = \sum_{i=1}^{N} \langle \psi_i(\mathbf{r}, t)|\mathbf{r}|\psi_i(\mathbf{r}, t)\rangle. \quad (5)$$

According to the Ehrenfest theorem [61], the time-dependent dipole acceleration $\boldsymbol{a}(t)$ of the system can be expressed as

$$\boldsymbol{a}(t) = \frac{d^2}{dt^2}\boldsymbol{d}(t) = \sum_{i=1}^{N} \langle \psi_i(\mathbf{r}, t)|-\nabla V_{\text{KS}}|\psi_i(\mathbf{r}, t)\rangle. \quad (6)$$

The harmonic spectrum can be produced by Fourier transform of time-dependent dipole acceleration [62]

$$H(\omega) = \left|\frac{1}{T_{\text{total}}}\int_0^{T_{\text{total}}} \boldsymbol{a}(t)e^{-i\omega t}dt\right|^2, \quad (7)$$

where T_{total} is the total duration of the laser pulse.

The ultrashort attosecond pulse can be generated by choosing harmonic coherent superposition in a certain energy range. The time-dependent intensity of the attosecond pulse can be expressed as

$$I(t) = \left|\int_{\text{q}} \boldsymbol{a}_q e^{iq\omega_0 t}\right|^2, \quad (8)$$

where q is the order of harmonics, $\boldsymbol{a}_q$ is

$$\boldsymbol{a}_q = \int \boldsymbol{a}(t)e^{-iq\omega_0 t}dt. \quad (9)$$

For investigating the behavior of HHG in the time domain, we use Molet time-frequency analysis [63]

$$A_\omega(t_0, \omega_0) = \int_{t_i}^{t_f} \boldsymbol{a}(t)w_{t_0,\omega}(t)dt, \quad (10)$$

where $w_{t_0,\omega}(t)$ is the kernel of the wavelet transform

$$w_{t_0,\omega}(t) = \sqrt{\omega}W[\omega(t - t_0)], \quad (11)$$

where

$$W(x) = \frac{1}{\sqrt{\tau}}e^{ix}e^{-x^2/2\tau^2}. \quad (12)$$

III. RESULTS AND DISCUSSION

A linearly polarized laser pulse is chosen in the simulation

$$\mathbf{E}(t) = E_0\left[\sin^2\left(\frac{\pi t}{T}\right)\right]\sin(\omega_0 t + \varphi)\hat{\mathbf{e}}_{\text{X}}. \quad (13)$$

The envelope of the electric field is the sin square one, and the peak amplitude of the pulse $E_0 = 0.09$ a.u.($I = 2.84 \times 10^{14}$ W/cm^2), the center frequency $\omega_0 = 0.057$ a.u. (the wavelength $\lambda = 800$ nm), the carrier-envelope phase $\varphi = 0$, the duration T is two optical cycles (o.c.). In the simulation, the molecular axis was chosen as the X axis along the polarization direction of the laser electric field. The nucleus is fixed, and the maximum internuclear distance of C_9H_{18}, C_4H_6 and BF molecules are 11.61, 5.41, Å and 1.26 Å, respectively. The calculated highest occupied molecular orbital (HOMO) energies of C_9H_{18}, C_4H_6 and BF molecules are -7.88 eV, -9.30 eV, and -11.15 eV, respectively. Experimentally, a weak alignment laser pulse can be applied, when the collimation effect is maximized, a linearly polarized driving laser is used to interact with the molecule. The HHG spectra of C_9H_{18}, C_4H_6, and BF molecules with similar ionization potential (I_P) irradiated by the laser pulse are shown in Fig. 1. It can be seen from Fig. 1 that, under the same laser pulse, the harmonic spectrum plateau of the C_9H_{18} molecule is wider and the cutoff is about ten orders larger than that of the BF molecule. The harmonic efficiency and the cutoff frequency of the C_9H_{18} spectrum are higher than those of the BF molecule. In the low-energy region(<30 harmonic orders) of the harmonic spectrum, the intensity of the C_9H_{18} is 2–3 orders higher than that of the BF molecule. In the high-energy region (>30 harmonic orders), the supercontinuum harmonic spectrum of the C_9H_{18} can be observed. The harmonic spectrum plateau of the C_4H_6 molecule is also extended. The harmonic emission efficiency and cutoff frequency of the C_4H_6 molecule are both between the C_9H_{18} molecule and the BF molecule. The harmonic efficiency of the C_4H_6 molecule is about one order higher than the BF molecule, and the cutoff frequency of the C_4H_6 molecule is about five orders higher than the BF molecule. There is obvious advantage on the harmonic intensity and cutoff frequency for long-chain molecules. The larger the molecular size is, the more the number of atoms is, and the more obvious the advantage is. It is worth noting that due to the small I_P of C_9H_{18}, C_4H_6, and BF molecules, the molecules have a chance to be ionized at the rising edge of the driving laser pulse, and harmonic spectra with larger cutoff energy cannot be obtained. The laser pulses used in this paper are ultrashort pulses and the interaction time between the laser and the molecule is very short, so the overall ionization is not large (the maximum ionization of a single electron orbital of C_9H_{18}, C_4H_6, and BF molecules are 0.182,

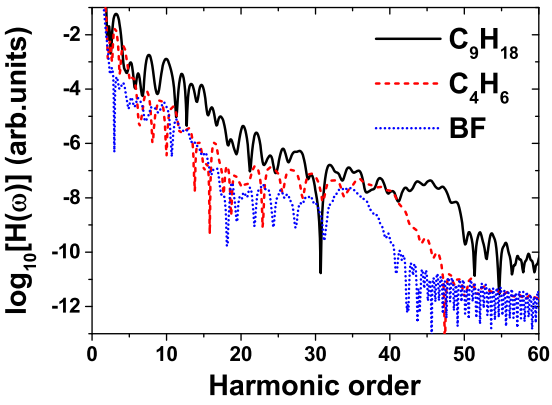

FIG. 1. The HHG spectra of C_9H_{18} (black solid line), C_4H_6 (red dashed line), and BF (blue dotted line). The electric field is polarized along the molecular axis $I = 2.84 \times 10^{14}$ W/cm^2, $\lambda = 800$ nm, $\varphi = 0$.

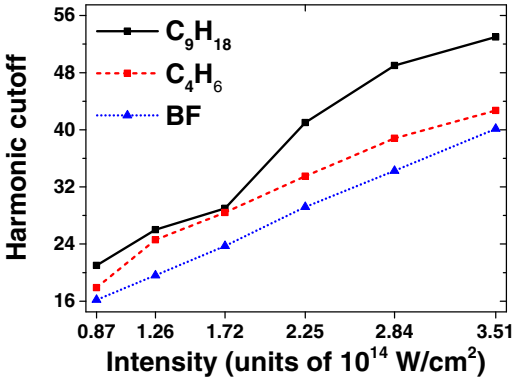

FIG. 2. The dependence of the harmonic cutoff frequency with the peak intensity of the laser pulse for C_9H_{18} (black circle), C_4H_6 (red square), and BF (blue triangle) molecules.

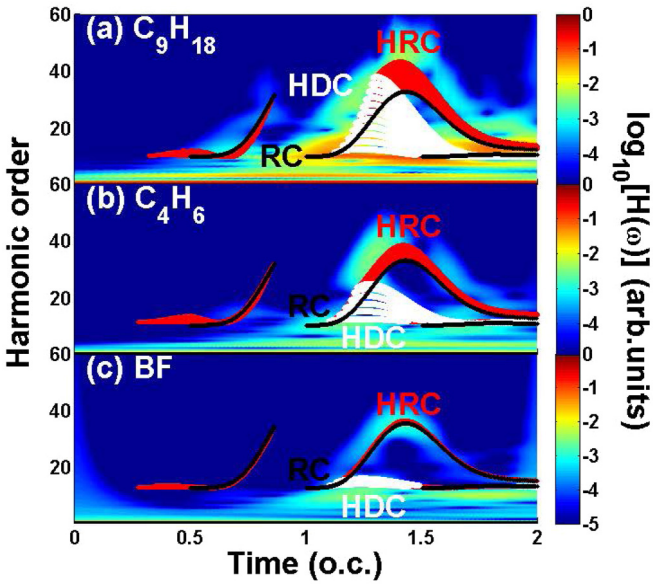

FIG. 3. Time-frequency behavior (color image) and classical analysis (curves) for the harmonic spectra from (a) C_9H_{18}, (b) C_4H_{16}, and (c) BF. Classical trajectory analysis is divided into three categories. The black curve represents the calculation result for ignoring the spatial scale of the molecule, which corresponds to the RC mechanism. When considering the spatial scale of the molecule, the red and white curves correspond to the HRC and HDC mechanisms, respectively. The parameters of the driving laser pulse are the same as Fig. 1.

0.233, and 0.245, respectively). Therefore, I_P has little effect on HHG. To understand the mechanism of the extension of the cutoff frequency and the harmonic intensity enhancement, we systematically investigated the influence of the driving laser intensity on the cutoff energy of the harmonic spectrum.

Figure 2 presents the change of the cutoff frequency with the peak amplitude of the laser electric field for C_9H_{18}, C_4H_6, and BF molecules. It can be seen from Fig. 2 that, for different electric laser intensity (from 0.87×10^{14} W/cm^2 to 3.51×10^{14} W/cm^2), the harmonic cutoff frequency of C_9H_{18} and C_4H_6 molecules are always greater than that of the BF molecule,and the harmonic cutoff frequency of the C_4H_6 molecule is always in between. As the intensity of the laser pulse increases, the difference between the cutoff frequencies from C_9H_{18}, C_4H_6, and BF molecules become larger. The harmonic cutoff frequency of the BF molecule can be predicted by the semi-classical three-step model [64], that is, electrons are ionized by the laser electric field, then return to the ionized region, and recombine with the parent ion to emit photons. For the C_9H_{18} and C_4H_6 molecules, they should need to further study the enhancement of the harmonic cutoff. In the following, we use the wavelet transform to analyze the time-frequency behavior of the molecular harmonic emission.

Figure 3 exhibits the time-frequency analysis of the harmonic spectra from C_9H_{18} and BF molecules. It can be seen from the figure that the harmonic emission of the two molecules mainly occurs within 1–2 o.c., C_9H_{18} molecular harmonics can be observed at 0.5–1o.c., and there is no harmonic generation for the BF molecules during this duration. To understand the behavior of HHG, the three-step model is applied to classically calculate the change of the harmonic energy with the recombination time. In the classical simulation, we first consider that electrons ionize from an atom, then move in the action of laser electric field, and come back this atom to emit harmonic photons. We call this process the return collision (RC) mechanism. Figure 3 shows the dependence of the harmonic order with the emission instant (black curve) in this mechanism. It can be noticed that, for the BF molecule, the classical harmonic emission behavior (black solid line) is consistent with that of the quantum calculation in the duration from 1 o.c. to 2 o.c., as shown by Fig. 3(b). However, the harmonic emission of C_9H_{18} from the quantum simulation is different from the classical trajectory (back solid curve), as presented in Fig. 3(a).

To clarify the difference between quantum and classical simulations of the C_9H_{18} HHG, we further considered the influence of the spatial effect on the C_9H_{18} harmonic spectrum. Figure 4 shows the structure of the C_9H_{18} molecule. The position of the C = C double bond is called the "head" and the position of methyl is called the "tail." At the instant t_1, many of the electrons are ionized in the "head" by the laser pulse and go forward along the X axis. When the electric field is reversed, it moves in the opposite direction. At the time t_2, a part of the returned electrons recollide with atoms in the head and radiate HHG, which is the RC mechanism. The returned electronic wave packet also has the opportunity to continue to be accelerated and may collide with atoms in the "tail" at the instant t_3, which is called heteronuclear return collision mechanism (HRC, as shown in the red curve in Fig. 4). In addition to the above two mechanisms, due to the larger spatial structure of the C_9H_{18} molecule, the electronic ionization can occur at the "head" at the time t_2, and electrons may move directly from one side of the molecule to the other under the action of the driving laser field, and emit harmonic photons at the instant t_3, which is called the heteronuclear direct collision mechanism (HDC, as presented by the blue curve in Fig. 4) [65].

Based on the HRC mechanism, the dependence of the harmonic energy with the recollision time is exhibited in the red curve in Fig. 3. It can be observed from this figure that, due to the small nuclear distance of the BF molecule, the result

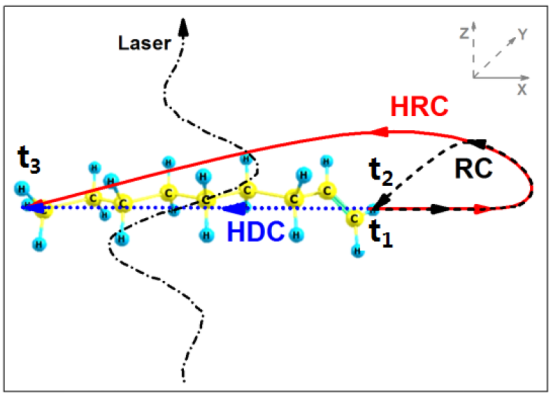

FIG. 4. Schematic diagram of the HHG mechanism of C_9H_{18}. The black dotted dashed line represents the laser electric field polarized along the molecular axis and the arrowed curve represents the movement of ionized electrons in the laser electric field. The harmonic emission time t_2 of the RC mechanism (black dashed line with arrow) originates from the ionization time t_1. Two ionization moments t_1 and t_2 lead to the same harmonic emission time t_3, which correspond to HRC (red solid line with arrow) and HDC mechanisms (blue dotted line with arrow), respectively.

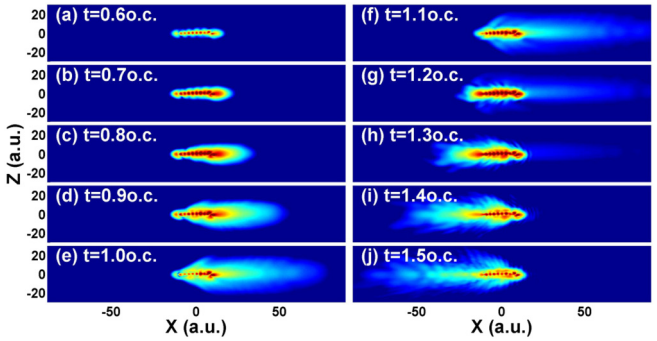

FIG. 5. Time-dependent evolution of the ionized electronic probability of C_9H_{18}. (a)–(j) corresponds to different instants $t = 0.6$ o.c. to $t = 1.5$ o.c., and the time interval $\Delta t = 0.1$ o.c. The lasers' parameters are the same as Fig. 1.

given by the HRC mechanism is the same as the case from RC. However, the two curves from HRC and RC for C_9H_{18} are quite different. The cutoff frequency of the harmonic spectrum from RC is about the 30th, while the maximum harmonic cutoff from HRC is about the 45th because of the large spatial scale of the C_9H_{18} molecule, which is close to the behavior of HHG on the space and timescale resolution in the quantum calculation. More importantly, it can be found that the harmonic spectrum from HRC is consistent with the classical calculation in the duration of 0.5 o.c. to 1 o.c.. In Fig. 3, we also presented the change of the harmonic order with the recombination instant (the white curve) from the HDC mechanism. By observing the time-frequency distribution of the C_9H_{18} HHG, it is noticed that the corresponding emission instants of 20 to 40th harmonics are around 1 o.c. to 1.5 o.c., there exists an interference structure. Because HDC and HRC contribute to harmonics in this emission region, which results in the interference structure of the C_9H_{18} harmonic spectrum. For the long-chain molecule C_4H_6, it can be seen from Fig. 3(b) that its harmonic emission mechanism is the same as that of the C_9H_{18} molecule, and the main reason for the increase in the cutoff frequency of its harmonic spectrum is the HRC mechanism, and the role of HDC mechanism also exists. The classical simulation of the harmonic is inconsistent with the quantum calculation results, so the role of RC mechanism alone cannot explain its harmonic emission mechanism. Since the long-chain molecules C_4H_6 and C_9H_{18} are only different in molecular size, the harmonic emission mechanism is the same. Therefore, the following research in this paper mainly focuses on the C_9H_{18} molecule, and the C_4H_6 molecule will not be repeated.

To visually observe the harmonic emission process of the C_9H_{18} molecule in the intense laser field, we calculated the time-dependent electron density of C_9H_{18} as a function of the time. Figures 5(a) to 5(j) present the electron probability density distribution from t =0.6 o.c. to $t = 1.5$ o.c., and the time interval $\Delta t = 0.1$ o.c. It can be seen from Fig. 5(a) that, at the instant $t = 0.6$ o.c., the electrons are mainly located near the nucleus because the intensity of the driving laser is wake. Driven by the laser electric field, the bound electrons are ionized and gradually move away from the molecular ions, then the electronic wave packets diffuse outward, as shown by Figs. 5(b) to 5(d). When the time reaches $t = 1.0$ o.c., the laser electric field is reversed. Because the electron has a larger velocity, its wave packet is still far away from the parent ion, as exhibited by Fig. 5(e). With the further increase of time, the electron wave packet moves in the opposite direction and returns to the parent ion, as presented by Figs. 5(f) to 5(g). It can also be seen from Figs. 5(h) to 5(j) that, under the action of the incident laser, the electrons of C_9H_{18} start to drive from the head to the tail and have the opportunity to collide with other nuclei of the molecule to release HHG through the HDC mechanism.

The harmonic spectrum of C_9H_{18} in the ultrashort laser pulse has a high intensity and shows a supercontinuum characteristic (the black solid line in Fig. 1), so it can be applied to generate isolated ultrashort pulses on the attosecond timescale with higher intensity. This part of the supercontinuum emission spectrum is filtered out, and a single attosecond pulse with the duration of 210 as can be obtained. On this basis, Figs. 6(a) and 6(b) display the influence of the CEP of the laser electric field on HHG and attosecond pulses, respectively. The CEP is ranged from 0 to 2π with an interval of $\pi/18$, and the resulting harmonic emission spectra are shown in Fig. 6(a). As can be observed from this figure, when CEP $= \pi/2$ and CEP $= 3\pi/2$, the cutoff frequencies of the harmonic spectra reach 60th order. When CEP $= 3\pi/4$, the harmonic cutoff is about 45th order. Filtering out the supercontinuous part of the harmonic spectra can produce isolated ultrashort attosecond pulses, as shown in Fig. 6(b). It can be seen from the figure that the CEP of the driving laser pulse has a strong modulation effect on the generation of the attosecond pulse. The attosecond pulse with the highest intensity is more than five orders of magnitude higher than the attosecond pulse with the smallest intensity, and the full width at half maximum (FWHM) of the attosecond pulse is also different. The intensity of isolated attosecond pulses in the CEP range of $5\pi/6$ to $3\pi/2$ is stronger and the corresponding FWHM is narrower.

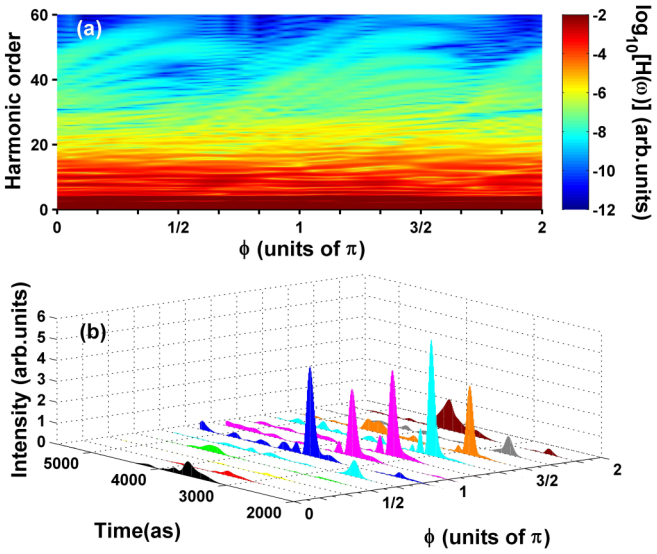

FIG. 6. (a) Harmonic spectra of C_9H_{18} at different CEPs, $\varphi = 0 \sim 2\pi$ (interval $\pi/18$); (b) attosecond pulses synthesized by supercontinuum harmonics from different CEPs, $\varphi = 0 \sim 2\pi$ (interval $\pi/6$). The other parameters of the laser pulse are the same as Fig. 1.

The obtained attosecond pulse at CEP $= 4\pi/3$ has the highest intensity and its FWHM is 108 as. To analyze the influence of the molecular orientation on the HHG, we presented the HHG spectra of C_9H_{18} molecule whose molecular axis varies from 0 to 2π respective to the polarization direction of the linearly polarized laser electric field, as shown in Fig. 7(a). It can be seen that there is harmonic emission from different orientation conditions and the intensity of harmonics in the low-energy region has little difference (10th to 30th orders), but there is a significant difference in the high-energy region (greater than the 30th order). When the direction of laser electric field is along the molecular axis, the cutoff energy of the harmonic spectra is the largest. As the orientation angles

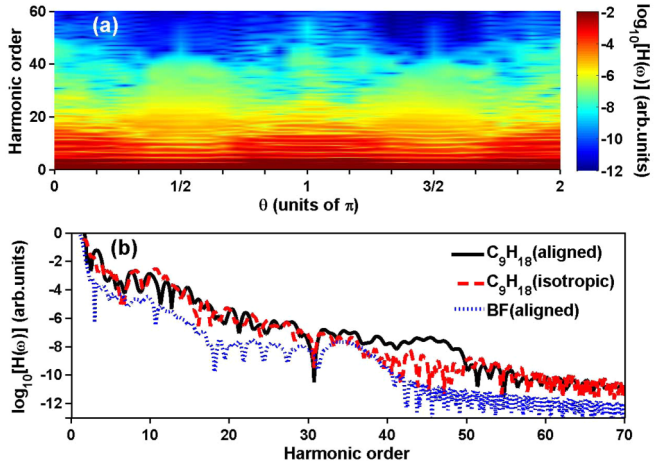

FIG. 7. (a) The HHG spectra of the C_9H_{18} molecule, the orientation angle $\theta = 0 \sim 2\pi$ (interval $\pi/18$). (b) The HHG spectra (black solid line) of the C_9H_{18} molecule when $\theta = 0$, the isotropic HHG spectrum (red dashed line) and the HHG spectrum (blue dotted line) of the BF molecule when $\theta = 0$.

are $\pi/2$ and $3\pi/2$ (the spatial size of the molecules along this direction is the smallest and the number of atoms is the smallest), the cutoff energy of the harmonic spectra is the smallest. According to the harmonic emission mechanism presented in Fig. 3 in the paper, under this condition, it can be known that the role of the HRC and HDC mechanisms on harmonic emission is smallest, and thus reducing largely the harmonic cutoff frequency. Figure 7(b) shows the high harmonic generated from the molecule which is isotropic or aligned. It can be seen from the figure that the cutoff frequency of the harmonic spectra is the same for the molecules which is isotropic or aligned. The intensity of the high-energy region (greater than 40th order) of the harmonic generated from the isotropic molecule is lower than the harmonic generated from the aligned molecule. Moreover, the harmonic intensity and cutoff frequency for C_9H_{18} molecule which is isotropic or aligned are both larger than that of the aligned BF molecule. Therefore, if a specific alignment pulse added in the experiment, the intensity and the maximum cutoff energy of HHG can be optimized.

IV. CONCLUSION

In conclusion, HHG of C_9H_{18} in the linearly polarized ultrashort laser pulse was investigated by using the TDDFT scheme. Compared with HHG of BF under the same laser field, it was found that the harmonic efficiency of C_9H_{18} is significantly higher and the cutoff energy of the harmonic spectrum is larger. Further studies demonstrated that the harmonic cutoff energy enhancement effect of C_9H_{18} exists for driving lasers with different intensities. Through the analysis of the harmonic time-frequency behavior and the electronic wave packet motion behavior of C_9H_{18}, it was verified that the electrons ionized from atoms at one side of the molecule recombined with atoms at the other side, which leads to the increase of the harmonic cutoff. The CEP of the ultrashort laser pulse has an apparent effect on the harmonic spectra and isolated attosecond pulses of C_9H_{18}, the higher intensity single attosecond pulse with 108 as can be generated. The orientation will affect the molecular harmonics. When the linearly polarized laser electric field is polarized along the molecular axis direction, the harmonic emission efficiency and cutoff frequency of the C_9H_{18} molecule are the higher.

In addition, we studied the HHG of the C_4H_6 molecule (a long-chain molecule whose molecular size is between C_9H_{18} and BF molecules), and found that the C_4H_6 molecule possesses the same harmonic emission mechanism as the C_9H_{18} molecule, and the efficiency and cutoff frequency of HHG spectra are significantly higher than the BF molecule. Our research reveals that the harmonic efficiency and the cutoff frequency can simultaneously be enhanced by using a complex molecule with a large spatial scale, which may pave the way to obtain a single attosecond pulse with higher intensity and shorter duration. We believe that the recombination mechanism discussed in this paper is generic for this molecular type. In future studies, we will try to find a long-chain molecule to enhance both the harmonic emission efficiency and the cutoff energy.

ACKNOWLEDGMENTS

This project was support by the National Key Research and Development Program of China (Grant No. 2019YFA0307700), National Natural Science Foundation of China (NSFC) (Grants No. 12074145, No. 11627807, and No. 11975012), Fundamental Research Funds for the Central Universities of China (Grant No. 30916011207), Outstanding Youth Project of Taizhou University (Grant No. 2019JQ002). We acknowledge the High Performance Computing Center of Jilin University for supercomputer time.

[1] C. H. K. M. Protopapas, and P. L. Knight, Rep. Prog. Phys. **60**, 389 (1997).

[2] G. G. Paulus, W. Nicklich, H. Xu, P. Lambropoulos, and H. Walther, Phys. Rev. Lett. **72**, 2851 (1994).

[3] A. l'Huillier, L. A. Lompre, G. Mainfray, and C. Manus, Phys. Rev. A **27**, 2503 (1983).

[4] D. Wu, F-M. Guo, J.-G. Chen, J. Wang, and Y-J. Yang, J. Phys. B: At. Mol. Opt. Phys. **53**, 235601 (2020).

[5] C. Wu, C. Wu, D. Song, H. Su, Y. Yang, Z. Wu, X. Liu, H. Liu, M. Li, Y. Deng, Y. Liu, L. Y. Peng, H. Jiang, and Q. Gong, Phys. Rev. Lett. **110**, 103601 (2013).

[6] J. Voigtsberger *et al.*, Nat. Commun. **5**, 5765 (2014).

[7] J. Itatani, J. Levesque, D. Zeidler, H. Niikura, H. Ppin, J. C. Kieffer, P. B. Corkum, and D. M. Villeneuve, Nature (London) **432**, 867 (2004).

[8] F. Krausz and M. Ivanov, Rev. Mod. Phys. **81**, 163 (2009).

[9] C. Vozzi, M. Negro, F. Calegari, G. Sansone, M. Nisoli, S. De Silvestri, and S. Stagira, Nat. Phys. **7**, 822 (2011).

[10] Y. Qiao, Y.-Q. Huo, S.-C. Jiang, Y.-J. Yang, and J.-G. Chen, Opt. Express **30**, 9971 (2022).

[11] J. Chen, Y. Yang, J. Chen, and B. Wang, Phys. Rev. A **91**, 043403 (2015).

[12] X. Cui, D-Y. Zhang, G. Chen, J.-G. Chen, S-L. Zeng, F-M. Guo, and Y-J. Yang, Chin. Phys. B **25**, 033205 (2016).

[13] D.-Y. Zhang, Q.-Y. Li, F.-M. Guo, and Y.-J. Yang, (in Chinese), Acta Phys. Sin. **65**, 223202 (2016).

[14] Y. Qiao, D. Wu, J.-G. Chen, J. Wang, F.-M. Guo, and Y.-J. Yang, Phys. Rev. A **100**, 063428 (2019).

[15] Y. Zhao, X. Xu, S. Jiang, X. Zhao, J. Chen, and Y. Yang, Phys. Rev. A **101**, 033413 (2020).

[16] Y.-T. Zhao, S.-C. Jiang, X. Zhao, J.-G. Chen, and Y.-J. Yang, Opt. Lett. **45**, 2874 (2020).

[17] T. Popmintchev, M.-C. Chen, P. Arpin, M. M. Murnane, and H. C. Kapteyn, Nat. Photonics **4**, 822 (2010).

[18] E. Goulielmakis *et al.*, Science **320**, 1614 (2008).

[19] C. Jia, J. Wang, Q-Y. Li, F-M. Guo, J.-G. Chen, S-L. Zeng, and Y-J. Yang, Opt. Express **23**, 32222 (2015).

[20] J. Wang, G. Chen, S-Y. Li, D-J. Ding, J.-G. Chen, M. Guo, and J. Yang, Phys. Rev. A **92**, 033848 (2015).

[21] F. Krausz, Phys. Scr. **91**, 063011 (2016).

[22] Y. Pan, F. Guo, C. Jin, Y. Yang, and D. Ding, Phys. Rev. A **99**, 033411 (2019).

[23] P. B. Corkum, Phys. Rev. Lett. **71**, 1994 (1993).

[24] J. Itatani, D. Zeidler, J. Levesque, M. Spanner, D. M. Villeneuve, and P. B. Corkum, Phys. Rev. Lett. **94**, 123902 (2005).

[25] N. A. Nguyen and A. D. Bandrauk, Phys. Rev. A **73**, 032708 (2006).

[26] F. H. M. Faisal, A. Abdurrouf, K. Miyazaki, and G. Miyaji, Phys. Rev. Lett. **98**, 143001 (2007).

[27] X. Ren and T. Nakajima, Phys. Rev. A **85**, 023403 (2012).

[28] Z. Diveki *et al.*, Chem. Phys. **414**, 121 (2013).

[29] E. Irani and M. Monfared, Chem. Phys. Lett. **719**, 27 (2019).

[30] Y. Pan, S.-F. Zhao, and X.-X. Zhou, Phys. Rev. A **87**, 035805 (2013).

[31] E. F. Penka, E. Couture-Bienvenue, and A. D. Bandrauk, Phys. Rev. A **89**, 023414 (2014).

[32] E. F. Penka and A. D. Bandrauk, Can. J. Chem. **90**, 616 (2012).

[33] A. Rupenyan, P. M. Kraus, J. Schneider, and H. J. Wörner, Phys. Rev. A **87**, 031401(R) (2013).

[34] K. Doblhoff-Dier, M. Kitzler, and S. Gräfe, Phys. Rev. A **94**, 013405 (2016).

[35] M. Monfared, E. Irani, and R. Sadighi-Bonabi, J. Chem. Phys. **148**, 234303 (2018).

[36] M. Ruberti, P. Decleva, and V. Averbukh, Phys. Chem. Chem. Phys. **20**, 8311 (2018).

[37] H. Yun, K. M. Lee, J. H. Sung, K. T. Kim, H. T. Kim, and C. H. Nam, Phys. Rev. Lett. **114**, 153901 (2015).

[38] C. Altucci, R. Velotta, E. Heesel, E. Springate, J. P. Marangos, C. Vozzi, E. Benedetti, F. Calegari, G. Sansone, S. Stagira, M. Nisoli, and V. Tosa, Phys. Rev. A **73**, 043411 (2006).

[39] N. Kajumba, R. Torres, J. G. Underwood, J. S. Robinson, S. Baker, J. W. G. Tisch, R. D. Nalda, W. A. Bryan, R. Velotta, C. Altucci, I. Procino, I. C. E. Turcu, and J. P. Marangos, New J. Phys. **10**, 025008 (2008).

[40] R. Torres, N. Kajumba, J. G. Underwood, J. S. Robinson, S. Baker, J. W. G. Tisch, R. de Nalda, W. A. Bryan, R. Velotta, C. Altucci, I. C. E. Turcu, and J. P. Marangos, Phys. Rev. Lett. **98**, 203007 (2007).

[41] C. Vozzi, R. Torres, M. Negro, L. Brugnera, T. Siegel, C. Altucci, R. Velotta, F. Frassetto, L. Poletto, P. Villoresi, S. De Silvestri, S. Stagira, and J. P. Marangos, Appl. Phys. Lett. **97**, 241103 (2010).

[42] X. Zhu, X. Liu, P. Lan, D. Wang, Q. Zhang, W. Li, and P. Lu, Opt. Express **24**, 24824 (2016).

[43] K.-J. Yuan, H. Lu, and A. D. Bandrauk, Phys. Rev. A **92**, 023415 (2015).

[44] A.D. Bandrauk, S. Chelkowski, H. Yu, and E. Constant, Phys. Rev. A **56**, R2537 (1997).

[45] M. Lein and J. M. Rost, Phys. Rev. Lett. **91**, 243901 (2003).

[46] G. Sansone, Phys. Rev. A **79**, 053410 (2009).

[47] F. Calegari, M. Lucchini, K. S. Kim, F. Ferrari, C. Vozzi, S. Stagira, G. Sansone, and M. Nisoli, Phys. Rev. A **84**, 041802(R) (2011).

[48] L. Cui *et al.*, Appl. Phys. Lett. **89**, 211103 (2006).

[49] A. Wardlow and D. Dundas, Phys. Rev. A **93**, 023428 (2016).

[50] N. Klemke, N. Tancogne-Dejean, G. M. Rossi, Y. Yang, F. Scheiba, R. E. Mainz, G. Di Sciacca, A. Rubio, F. X. Kärtner, and O. D. Mücke, Nat. Commun. **10**, 1319 (2019).

[51] N. Tancogne-Dejean, O. D. Mücke, F. X. Kärtner, and A. Rubio, Nat. Commun. **8**, 745 (2017).

[52] F. Bedurke, T. Klamroth, and P. Saalfrank, Phys. Chem. Chem. Phys. **23**, 13544 (2021).
[53] M. A. L. Marques, A. Castro, G. F. Bertsch, and A. Rubio, Comput. Phys. Commun. **151**, 60 (2003).
[54] A. Castro, H. Appel, M. Oliveira, C. A. Rozzi, X. Andrade, F. Lorenzen, M. A. L. Marques, E. K. U. Gross, and A. Rubio, Phys. Status Solidi B **243**, 2465 (2006).
[55] X. Andrade, D. Strubbe, U. De Giovannini, A. H. Larsen, M. J. Oliveira, J. Alberdi-Rodriguez, A. Varas, I. Theophilou, N. Helbig, M. J. Verstraete, L. Stella, F. Nogueira, A. Aspuru-Guzik, A. Castro, M. A. Marques, and A. Rubio, Phys. Chem. Chem. Phys. **17**, 31371 (2015).
[56] E. Runge and E. K. U. Gross, Phys. Rev. Lett. **52**, 997 (1984).
[57] N. Troullier and J. L. Martins, Phys. Rev. B **43**, 1993 (1991).
[58] J. P. Perdew, K. Burke, and M. Ernzerhof, Phys. Rev. Lett. **77**, 3865 (1996).
[59] A. Castro, M. A. Marques, and A. Rubio, J. Chem. Phys. **121**, 3425 (2004).
[60] U. De Giovannini, A. H. Larsen, and A. Rubio, Eur. Phys. J. B **88**, 56 (2015).
[61] I. Tavernelli, U. F. Röhrig, and U. Rothlisberger, Mol. Phys. **103**, 963 (2005).
[62] A. Castro, A. Rubio, and E. K. U. Gross, Eur. Phys. J. B **88**, 191 (2015).
[63] P. Goupillaud, A. Grossmann, and J. Morlet, Geoexploration **23**, 85 (1984).
[64] M. Lewenstein, P. Balcou, M. Y. Ivanov, A. L'Huillier, and P. B. Corkum, Phys. Rev. A **49**, 2117 (1994).
[65] J. Wang, G. Chen, F.-M. Guo, S.-Y. Li, J.-G. Chen, and Y.-J. Yang, Chin. Phys. B **22**, 033203 (2013).